Contrib Mineral Petrol (2008) 155:79–92
DOI 10.1007/s00410-007-0226-4

ORIGINAL PAPER

Li-Sr-Nd isotope signatures of the plume and cratonic lithospheric mantle beneath the margin of the rifted Tanzanian craton (Labait)

Sonja Aulbach · Roberta L. Rudnick · William F. McDonough

Received: 10 October 2006 / Accepted: 29 May 2007 / Published online: 17 July 2007

Abstract Lithium concentrations and isotopic compositions of olivine and $^{87}Sr/^{86}Sr$ and $^{143}Nd/^{144}Nd$ of coexisting clinopyroxene from peridotite xenoliths from the Quaternary Labait volcano, Tanzania, document the influence of rift-related metasomatism on the ancient cratonic mantle. Olivines show negative correlations between Fo content and both δ^7Li and Li concentrations. Olivines in iron-rich peridotites ($Fo_{85–87}$) have high Li concentrations (3.2–4.8 ppm) and heavy δ^7Li (+5.2 to +6.6). In contrast, olivines in ancient, refractory peridotites have lower Li concentrations (~2 ppm) and relatively light δ^7Li (+2.6 to +3.5). This reflects mixing between ancient, refractory cratonic lithosphere and asthenosphere-derived rift magmas. A uniquely fertile, deformed, high-temperature garnet lherzolite, interpreted to be from the base of the lithosphere, has a $^{87}Sr/^{86}Sr$ of 0.7029 and $^{143}Nd/^{144}Nd$ of 0.51286, similar to HIMU oceanic basalts. It provides the best estimate of the Sr–Nd isotope composition of the upwelling mantle (i.e., plume, sensu lato) underlying this portion of the East African Rift, and is slightly less radiogenic compared to previous estimates of the plume that were based on rift basalts. Although elevated δ^7Li are not exclusive to HIMU source regions, the data collectively indicate that the plume beneath Labait has HIMU characteristics in Sr, Nd and Li isotope composition.

Keywords Lithium isotopes · Strontium isotopes · Neodymium isotopes · East African Rift · Plume · Cratonic lithospheric mantle · Tanzania

Communicated by J. Hoefs.

Electronic supplementary material The online version of this article (doi:10.1007/s00410-007-0226-4) contains supplementary material, which is available to authorized users.

S. Aulbach · R. L. Rudnick · W. F. McDonough
Geochemistry Laboratory, Department of Geology, University of Maryland, College Park, MD 20742, USA

Present Address:
S. Aulbach (✉)
Earth and Atmospheric Sciences, University of Alberta, Edmonton, AB T6G 2E3, Canada
e-mail: aulbach@ualberta.ca

Introduction

Xenolithic peridotites carried in rift-related alkali basalts from Tanzania offer a unique opportunity to investigate the effects of rifting and intrusion of rift-related melts on cratonic subcontinental lithospheric mantle (SCLM) that has experienced multiple previous enrichment episodes (Dawson 1984, 1999, 2002; Rudnick et al. 1992, 1993; Lee and Rudnick 1999; Chesley et al. 1999; Vauchez et al. 2005). The East African Rift (EAR) is widely attributed to the impingement of a plume or plumes (sensu lato) that delivered heat and fluids to the lithospheric mantle, leading to its thinning and enrichment in incompatible elements. Evidence for plume involvement includes the similarity of some EAR magmas to ocean island basalts (OIBs) (e.g., Marty et al. 1996; Bell and Simonetti 1996; George et al. 1998; Rogers et al. 2000), radiogenic Os isotopes in mantle xenoliths precipitated by rift magmas (Chesley et al. 1999), the volume of extruded and underplated melts (Latin et al.

1993) and geophysical data (e.g., Ebinger et al. 1989; Weeraratne et al. 2003).

Although it is postulated that plumes should exhibit a range of Li isotopic compositions, since they may contain deeply subducted slabs consisting of variably altered and dehydrated oceanic crust and mantle with distinct δ^7Li (Li isotope composition relative to L-SVEC standard: $\{[(^7Li/^6Li)_{sample}/(^7Li/^6Li)_{L\text{-}SVEC} - 1] \times 1{,}000\}$ Chan et al. 1992, 2002; Zack et al. 2003; Nishio et al. 2004, 2005; Wunder et al. 2006), a direct connection between the lithium isotope composition of intraplate basalts and inferred slab components is yet to be established. Most OIBs have δ^7Li overlapping with MORB (δ^7Li = +2 to +6, see Ryan and Kyle (2004) and references therein), but a few OIBs and associated glasses have δ^7Li trending toward both heavier and lighter δ^7Li values (Gurenko and Schmincke 2002; Kobayashi et al. 2004; Ryan and Kyle 2004; Nishio et al. 2005). In particular, the δ^7Li of the HIMU source has been suggested to be heavier than MORB (+6 to +7), either due to incorporation of slab-modified isotopically heavy mantle wedge materials (Jeffcoate and Elliott 2003) or incorporation of less altered (and hence, less dehydrated) oceanic crust (Nishio et al. 2005). In contrast, highly altered and dehydrated basaltic crust and pelagic sediment have been suggested to give rise to low δ^7Li in the EMI source [inferred from unusually light Li in clinopyroxenes from mantle xenoliths from far-east Russia and SW Japan (Nishio et al. 2004)], although the basis of this interpretation has been recently questioned (Jeffcoate et al. 2007; Rudnick and Ionov 2007).

Volcanic rocks in the EAR have trace-element and isotopic compositions comparable to those of OIBs, but occupy a unique field in isotope compositional space compared to OIBs (Paslick et al. 1995; Rogers et al. 2000; Macdonald et al. 2001). Part of this uniqueness may stem from their interaction with the ancient, incompatible trace element-enriched lithospheric mantle. Rogers et al. (2000) suggest that the present-day plume has Sr and Nd isotope compositions of 0.7035 and 0.51275, respectively, which is the isotopic composition of the common end-member of Neogene to Recent Kenya rift basalts.

We report here the Li, Sr and Nd isotope and trace-element compositions of minerals from peridotite xenoliths from the Labait volcano, which erupted on the margin of the Archean Tanzanian craton. These data are used to determine the effects of the rift-related magmas on the Li, Sr and Nd isotope composition of the cratonic lithospheric mantle and to gain further insights into the composition of the plume that is feeding magmas of the EAR. These xenoliths have been the subject of previous detailed petrographic, major- and trace-element and Re-Os isotope investigations that documented heating and intrusion of the ancient lithosphere by rift-related melts (Dawson 1999; Lee and Rudnick 1999; Chesley et al. 1999).

Geology

The Gregory rift, the eastern branch of the EAR system in Tanzania, cuts along the border between the Archean Tanzanian craton and the Mozambique fold belt to the east. The latter is composed largely of Archean crust that was reworked in at least two Proterozoic orogenies, the ~2.1 Ga Usagaran orogeny and the ~600 Ma pan-African orogeny (Möller et al. 1998). Earliest manifestations of volcanic activity in the EAR system date back to 50–30 Ma in Kenya and the magmatic activity has moved southward since the mid Tertiary, leading to magmatism in Tanzania between 1 and 5 Ma (Dawson 1992). Voluminous basaltic to trachytic magmatism, forming large shield volcanoes in the mobile belt, was followed by faulting at about 1.2 Ma and eventually small-volume explosive, highly alkaline nephelinitic to carbonatitic volcanism, which is restricted to the craton and reworked craton margin (Dawson 1992; Smith and Mosley 1993) where the Labait volcano erupted.

The olivine–melilitite that forms the Labait volcano marks the southernmost point of the propagating Gregory Rift, where rifting is incipient (Dawson 1999). It sampled the SCLM beneath the eastern edge of the Tanzanian craton in the form of relatively large mantle xenoliths (Lee and Rudnick 1999). The volcano was indirectly dated to ca <0.4 Ma on the basis of U-Pb ages of metasomatic zircons in one of the peridotite xenoliths (Rudnick et al. 1999).

The mantle lithosphere beneath Labait is highly refractory to depths of ~140 km, and shows a stepwise increase in fertility between 140 and 150 km (Lee and Rudnick 1999). Re-Os ages up to 2.9 Ga in peridotitic chromites from the upper 140 km of mantle lithosphere indicate stabilization by the Late Archean and testify to its longevity, despite the propagation of the rift into the craton; Proterozoic to future Os model ages for peridotites from the deeper, garnet-bearing, more fertile lithosphere may indicate later formation (i.e., in the Proterozoic) or modification of Archean lithosphere by interaction with the EAR magmas (Chesley et al. 1999). Multiple lines of evidence attest to intrusion and heating of the ancient lithosphere by rift-related magmas. These include: (a) breakdown of garnets into coronas (Lee and Rudnick 1999), (b) the presence of metasomatic veins containing more Fe-rich olivine, phlogopite, orthopyroxene, chromite, sulfide, 400 Ka zircons (Rudnick et al. 1999) and rutile with enhanced Zr concentrations on the rims, indicative of heating (Watson et al. 2006) and (c) recent Re addition (Chesley et al. 1999; Burton et al. 2000). Seismic signatures from the craton margin are transitional between

lithospheric (in terms of anisotropy) and asthenospheric (in terms of seismic velocities) mantle, suggesting that the base of the lithosphere has been modified by a plume, which is likely responsible for the rifting (Vauchez et al. 2005).

Samples

Xenoliths from Labait can be divided into garnet-bearing peridotites, chromite-bearing garnet-free peridotites (containing chrome-rich spinel and Al_2O_3-poor opx typical of garnet-facies peridotites, but do not contain garnet) and spinel-facies peridotites (containing aluminous spinel and Al_2O_3-rich opx; Lee and Rudnick 1999; see also key parameters in Supplementary Appendix 1). Most also contain glassy pockets or veins (Dawson 1999). The mantle xenolith population is made up of >75% Fe-rich peridotites (of which ca 25% contain chrome diopside) and ca. 25% harzburgites or cpx-poor lherzolites, with rare glimmerites and wehrlites (Lee and Rudnick 1999). Olivine is fresh, with mosaic-porphyroclastic textures in garnet peridotites. Orthopyroxene forms small to large groundmass grains. Clinopyroxene displays well-developed morphology in wehrlites and garnet-bearing peridotites, and also occurs in garnet reaction rims and glassy patches, where it appears to be secondary. Garnet has mostly decomposed to kelyphite and an outer corona assemblage, with remnants occurring in the center of kelyphite. Olivine compositions may be heterogeneous, depending on habit and whether it occurs as inclusions or within the matrix. Olivine inclusions in garnet can have higher forsterite content than matrix olivines, reflecting Fe-enrichment post-dating garnet growth (Lee and Rudnick 1999).

Spinel-facies and garnet-free chromite-bearing peridotites are highly refractory (FeO = 6.5–7.4 wt%), whereas most garnet-bearing peridotites are more fertile, though still depleted relative to estimates for the primitive upper mantle composition (FeO = 7.6 to 10.6 wt%; Lee and Rudnick 1999). In contrast, Fe-rich peridotites (FeO = 11.2 to 14.1 wt%) are olivine-rich and have been interpreted as products of pervasive melt-rock reaction, rather than cumulates, on the basis of their significant Os concentrations (e.g., 0.9–2.9 ppb, Chesley et al. 1999). Garnet lherzolite LB-45 is unique in that it is derived from near the lithosphere–asthenosphere boundary at a temperature of ca 1,400°C, has a major element composition similar to primitive upper mantle estimates (Lee and Rudnick 1999) and radiogenic Os isotopic composition (Chesley et al. 1999). Based on these features, Chesley et al. (1999) suggested that this sample may derive from the plume beneath the EAR. More recent PGE analyses of this sample, using a high-temperature Carius tube digestion technique (Becker et al. 2006), show that the whole rock $^{187}Os/^{188}Os$ is somewhat less radiogenic than measured by Chesley et al. (1999), who used lower-temperature Carius tube digestion. These differences show that there are at least two populations of Os in the sample: an ancient, unradiogenic component, presumably armored within chromites, and a radiogenic component that is presumably contained within more acid-accessible, late-stage sulfides. Moreover, its platinum group element concentrations are much lower than primitive mantle (PM) and are accompanied by anomalous Re-enrichment. These features suggest that this sample is probably a piece of the original, Archean cratonic mantle that was strongly overprinted by rift-related magmas (Becker et al. 2006) near the base of the lithosphere.

Sample preparation, chemistry and analytical methods

Mineral separates, hand-picked to optical purity and cleaned in Milli-Q (18 MΩ) H_2O in an ultrasonic bath for 15 min, were dissolved in a 3:1 mixture of concentrated HF–HNO_3 in Savillex screw-top beakers and dried down. The dried residua were replenished with HCl–HNO_3 mixture and HCl until clear solutions were obtained. The three-column chemistry for olivine is based on the procedure described by Moriguti and Nakamura (1998) and closely follows that described in Rudnick et al. (2004). Each column is loaded with Bio-Rad AG 50W-X12 (200–400 mesh) resin. Column calibrations using BHVO-1 as the low-Cr-Mg end of spectrum and a powdered peridotite as the high-Cr-Mg end were performed to ensure 100% yield for both types of matrix. In addition, the yield was monitored by taking aftercuts and measuring their Li contents on the Finnigan ELEMENT 2 magnetic sector Inductively Coupled Plasma Mass Spectrometer (ICPMS) in the Department of Geology at the University of Maryland. Analyses were rejected if more than 3% of Li was lost during any single column pass, which occurred during the processing of <10% of sample aliquots. Li loss was sporadic and could not be linked to differences in sample type or composition. Repeat analyses of samples in our dataset with up to 3% loss agreed within the analytical uncertainty.

Prior to Li isotope analysis, Na/Li was measured semi-quantitatively using voltage ratios obtained on the Nu Plasma Multi-Collector (MC) ICPMS at the University of Maryland, as ratios >5 are known to interfere with accurate Li isotope determination (Tomascak et al. 1999). Samples with Na/Li > 5 were dried down and passed a second time through column 3 to achieve greater Na–Li separation.

Purified Li solutions (~50 ppb Li in 2% (v/v) HNO_3) were carried by a mixture of Ar and N from an autosampler (ASX-100 Cetac Technologies) through a desolvating nebulizer (Aridus Cetac Technologies) fitted with a

PFA spray chamber and micro-nebulizer (Elemental Scientific) to the Nu plasma MC-ICPMS at the University of Maryland. The standard bracketing method described in Teng et al. (2004) was used. Lithium concentrations were determined by comparison of sample signal intensities with those obtained from L-SVEC, with a two sigma uncertainty of ~10%, as determined using isotope dilution methods (Teng et al. 2004).

The accuracy and precision of the data are assessed by repeated analysis of rock standards and the pure Li in-house standards Li-UMD-1 and of IRMM-016, with yielded average δ^7Li of +54.6 ± 0.8 (2σ, n = 27) and +0.2 ± 1.0 (2σ, n = 17), respectively, during the course of the analyses presented here. In general, external precision (2σ on repeat runs) is ≤1‰ based on long-term analyses of these standards (Teng et al. 2004), where isotopic compositions are expressed as per mil (‰) deviations from the NIST L-SVEC Li_2CO_3 standard. The δ^7Li for international rock standards agree within uncertainty with previously published values [note that serpentinite UB-N is the international standard with the closest matrix to our ultramafic samples (Supplementary Appendix 2)]. Total procedural blanks were always ≤400 pg Li (average 250 pg, n = 5) and blank contributions were, on average, ≤0.07% of the measured δ^7Li, which is insignificant compared to the external precision.

Clinopyroxene separates were spiked with a ^{150}Nd spike (99% abundance) prior to dissolution, which follows the procedure described above. Strontium and Nd cuts were obtained in two stages. In the first column, filled with Bio-Rad AG 50W-X12 (200–400 mesh) resin, Sr and Nd cuts were collected by eluting with 2.5 N HCl and 6.0 N HCl, respectively. Rb and Sr are separated quite efficiently during this first stage (total Rb in Sr cut = 0.2%). Nevertheless, a second-stage purification of the Sr cut was performed, using Eichrom Sr-SPEC resin. Separation of Nd from other REE was achieved with an Eichrom Ln-resin.

Strontium cuts were loaded on Re filaments with a Ta activator and isotope ratios measured in dynamic collection mode on the VG Sector 54 TIMS at the University of Maryland, using a ^{86}Sr/^{88}Sr of 0.1194 for mass fractionation correction. Multiple ^{87}Sr/^{86}Sr analyses of standards are reported in Supplementary Appendix 3.

Like lithium, purified Nd solutions were introduced into the Nu Plasma MC-ICPMS with an Aridus desolvating nebulizer. Neodymium isotope ratios were measured in static collection mode, where the collector configuration for Nd isotope analysis is such that all Nd isotopes plus ^{147}Sm are analyzed (to monitor interference of ^{144}Sm on ^{144}Nd), with mass 144 on the axial channel. Mass fractionation is corrected by normalizing to a ^{146}Nd/^{144}Nd of 0.7219. Multiple ^{143}Nd/^{144}Nd analyses of AMES Nd standard averaged 0.512191 ± 0.000027 (2σ, n = 44). Rock standards and samples were normalized to a ^{143}Nd/^{144}Nd for AMES of 0.512138 (in-house TIMS measurements). Using this method, average ^{143}Nd/^{144}Nd for Shin-Etsu is 0.512121 ± 0.000032 (n = 8) and for BHVO-1 it is 0.512989 ± 0.000039 (n = 4). A single analysis of BCR-1 gave 0.512601 ± 0.000024 (2s.e.) (Supplementary Appendix 3). The blank concentration was 9.3 ng and thus did not require a correction.

Trace-element abundances in cpx were determined using either a frequency-quintupled Nd:YAG laser operating at 213 nm or an ArF Excimer operating at 193 nm (both from New Wave Research), coupled to the ELEMENT 2. Helium was used as the sample gas. Laser spot sizes ranged from ~80 to 100 μm, at an 8–10 Hz laser repetition rate. A typical time-resolved analysis involved ~20 s of background acquisition on the sample gas, followed by laser ablation for 40 s. Each batch of ca 20 analyses was preceded and followed by analysis of standards NIST 610 and BCR-2g, the latter analyzed as an unknown (Supplementary Appendix 4). Absolute trace-element abundances were obtained after processing the time-resolved spectra off-line (using a modified version of LAMTRACE by Simon E. Jackson) including background subtraction and normalization to ^{49}Ti, based on analyses of Ti by electron microprobe (Lee and Rudnick 1999).

Results

Lithium concentrations for olivine separates from Labait range from 1.8 to 4.8 ppm and δ^7Li from +2.5 to +6.6 (Table 1). Lithium isotopic compositions of olivines correlate positively with Li concentration (Fig. 1a) and negatively with Fo and NiO contents (Fig. 2). Olivines in three Fe-rich peridotites have the heaviest Li (+5.2 to +6.6) and some of the highest Li concentrations (Fig. 1a), while at the other end of the spectrum, Li contents of olivines from the spinel and garnet-free chromite-bearing harzburgites are the lowest (~2 ppm) and they have the lightest δ^7Li (~+3). Olivines from all three garnet-bearing peridotites, including the fertile garnet lherzolite (LB-45), have identical Li isotopic compositions (δ^7Li = +4.7), which are intermediate between the Fe-rich peridotites and refractory harzburgites, and similarly intermediate Li concentrations (2.3–3.4 ppm).

In all but one sample (gt-free harzburgite LB-21), pyroxenes have lithium concentrations that are equal to or lower than those in coexisting olivines, with apparent $^{ol/cpx}$D (the concentration of Li in olivine divided by that in cpx) of 1.1–2.0, consistent with equilibrium partitioning (Table 1; Fig. 3, Brenan et al. 1998; Eggins et al. 1998; Seitz and Woodland 2000). The δ^7Li of the orthopyroxenes are equal to or lighter than that of coexisting olivines by up

Table 1 Lithium isotope compositions (‰), concentrations (ppm), apparent olivine–cpx distribution coefficients and inter-mineral fractionations (Δ^7Li), where applicable, for peridotitic mineral separates and the host melilitite

Sample	δ^7Li ol	Li ol	δ^7Li opx	Li opx	δ^7Li cpx	Li cpx	$^{ol/cpx}D$	Δ^7Li^{ol-cpx}	Δ^7Li^{ol-opx}
Spinel-facies harzburgites									
LB-29	3.3								
LB-29	4.0								
LB-29	4.5								
LB-29	3.6								
LB-29	2.5								
LB-29	2.8								
LB-29 ave	***3.4***	1.9	3.5	1.2					–0.1
LB-31	3.1								
LB-31	3.5								
LB-31 ave	***3.3***	1.8			1.5	0.9	2.0	1.8	
Garnet harzburgites and lherzolite									
KAT-17	4.8		2.7						
KAT-17	4.7		3.7						
KAT-17 ave	***4.7***	3.4	***3.2***	0.8	–0.3	2.2	1.5	5.0	1.5
LB-4			1.5						
LB-4			1.4						
LB-4	3.8		1.2		–2.2				
LB-4	5.6		0.5		–3.0				
LB-4 ave	***4.7***	2.3	***1.2***	1.2	***–2.6***	1.2	1.9	7.3	3.6
LB-45					–0.2				
LB-45					0.3				
LB-45 ave	***4.7***	2.4	0.7	2.5	***0.1***	2.0	1.2	4.6	4.0
Garnet-free harzburgites									
LB-6	4.3		–3.8						
LB-6	3.2		–4.5						
LB-6 ave	**3.7**	1.9	***–4.1***	1.9					7.9
LB-17	3.9								
LB-17	4.1								
LB-17 ave	***4.0***	2.7							
LB-21	3.8								
LB-21	1.3								
LB-21 ave	***2.5***	2.2	1.1	1.5	–4.9	3.8	0.6	7.4	1.4
Fe-rich peridotites									
LB-46	5.5								
LB-46	4.9								
LB-46 ave	***5.2***	4.4	–1.8	3.8	–6.7	3.0	1.5	11.9	
LB-51	6.8								
LB-51	6.3								
LB-51 ave	***6.6***	4.8			4.1	4.4	1.1	2.4	6.6
LB-59	6.9								
LB-59	6.3								
LB-59 ave	***6.6***	3.2							
Melilitite									
LB-2	5.1								
LB-2	4.8								
LB-2 ave	***5.0***	10.1							

LB21 ol reproduced within 1.2‰ uncertainty, all others within 1‰

Averages (ave) are given in bold italics

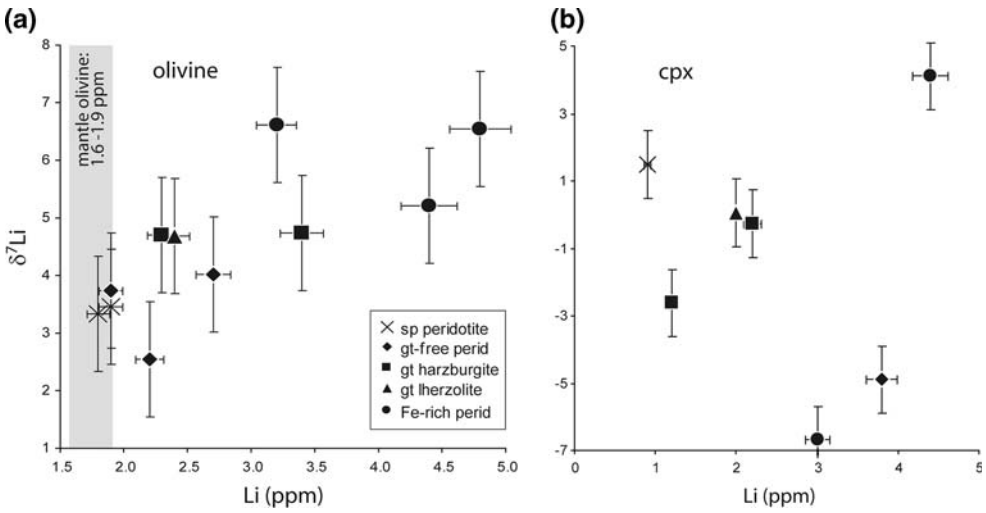

Fig. 1 δ^7Li (‰) against Li concentration (ppm) in **a** olivine (correlated with an r^2 of 0.59) and **b** cpx from Labait. *Error bars* are 1‰ and 10%, respectively. Estimate for range of Li contents in olivine from fertile to moderately depleted mantle from Eggins et al. (1998) and Seitz and Woodland (2000)

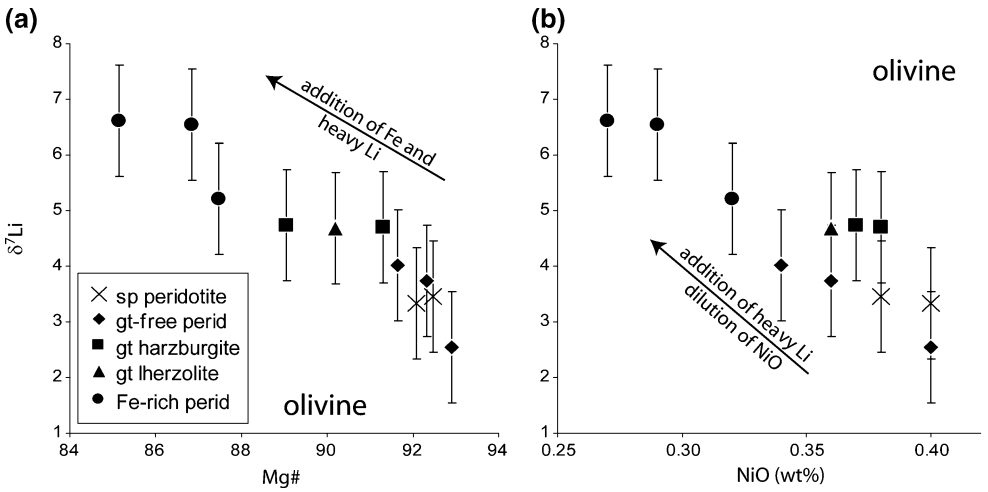

Fig. 2 **a** Mg-number [Mg number: 100Mg/(Mg + Fe)] against δ^7Li (‰) (correlated with an r^2 of 0.89) and **b** NiO (wt%) against δ^7Li (‰) (correlated with an r^2 of 0.80) for peridotitic olivine separates from Labait. Qualitative mixing trends for the addition of Fe and Li and dilution of NiO are also shown. Mg-numbers and NiO contents from Lee and Rudnick (1999)

to 7‰ and those of clinopyroxenes are consistently lighter than olivines by 2–12‰ (Fig. 3). These inter-mineral fractionations do not correlate with equilibration temperature and there is no correlation between δ^7Li, Li content and Mg number in clinopyroxenes (Fig. 1b).

Strontium isotope compositions for seven cpx separates range from 0.702945 in the fertile garnet lherzolite (LB-45) to 0.705584 in an Fe-rich peridotite (Table 2). Unfortunately, Nd was lost for some of these samples and there is not enough material left to attempt repeat measurements. Nevertheless, ε_{Nd} values for four cpx separates range from a low of –8.6 in a spinel peridotite to a high of +4.8 in an Fe-rich peridotite and an analytically indistinguishable value of +4.4 in the fertile garnet lherzolite, LB-45 (Table 2). δ^7Li_{ol} shows a rough negative correlation with $^{87}Sr/^{86}Sr$ (Fig. 4a, with one outlier), and a positive correlation with ε_{Nd} values in cpx (Fig. 4b), though the limited data make these correlations less than robust.

With the exception of the most incompatible elements, PM-normalized trace-element patterns of clinopyroxenes in the peridotites from Labait are mostly similar, with moderate, negative slopes in the REE ($LREE_N$ ~10–50, $HREE_N$ ~1–3) that flatten in the LREE (Supplementary Appendix 4, Fig. 5). The cpx in a garnet harzburgite (sample LB-4) has markedly lower incompatible trace-element concentrations, whereas that in a garnet-free chromite-bearing harzburgite (sample LB-21) has markedly higher incompatible trace-element abundances than the remainder of the samples. The latter sample shows extreme enrichment in Zr and Hf and is the only sample with Zr/Hf >PM and with $^{ol/cpx}D_{Li}$ <1; the rest have PM-normalized Zr/Hf <1 and $^{ol/cpx}D_{Li}$ >1. The

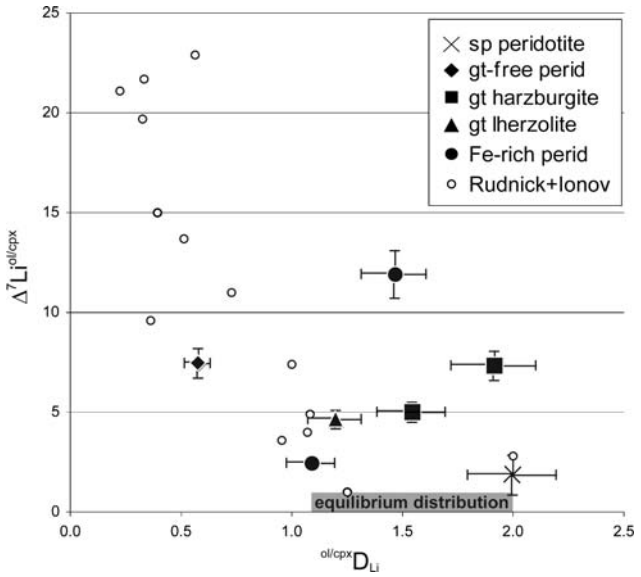

Fig. 3 Apparent olivine–cpx partitioning coefficients ($^{ol/cpx}D_{Li}$) plotted against inter-mineral Li isotope fractionation (Δ^7Li^{ol-cpx}). *Gray bar* shows range of equilibrium distribution coefficients (adapted from Eggins et al. 1998; Brenan et al. 1998; Seitz and Woodland 2000). Peridotites from far-east Russia (adapted from Rudnick and Ionov 2007) shown for comparison

similarity between the cpx patterns in garnet-bearing and garnet-free peridotites is surprising, considering that cpx is the only mineral into which these elements partition in the garnet-free samples, yet garnet should take in significant HREE when it is present. However, cpx in garnet-free samples do have significantly higher Sc concentrations than in garnet-bearing ones, suggesting that they are indeed garnet-free, as Sc is highly compatible in garnet.

Discussion

Li isotopic disequilibria

Lithium concentrations in both olivines and pyroxenes from the Labait peridotites range to significantly higher values than "normal" mantle, as defined by Seitz and Woodland (2000). These enrichments are evidence for Li addition to the samples some time after the melt depletion that they experienced in the Archean. With the exception of the very refractory harzburgite (LB-21), which has a low $^{ol/cpx}D_{Li}$ of 0.6, the $^{ol/cpx}D_{Li}$ values of the Labait peridotites fall within the range considered to reflect equilibrium partitioning ($^{ol/cpx}D_{Li}$ = 1.1–2.0, Brenan et al. 1998; Eggins et al. 1998; Seitz and Woodland 2000). This result is noteworthy, given that in many peridotites metasomatized by a silicate melt, cpx is preferentially, sometimes strongly, enriched in Li relative to olivine (Seitz and Woodland 2000; Paquin and Altherr 2002; Scambelluri et al. 2006; Rudnick and Ionov 2007), resulting in disequilibrium $^{ol/cpx}D_{Li}$ <1 (Fig. 3). In contrast, the rather large differences in Li isotopic compositions between coexisting olivine and pyroxene (Table 1 and Fig. 3), discussed below, show that they are not equilibrated with respect to Li isotope composition. Thus, isotopic disequilibrium exists despite apparent elemental equilibrium.

Table 2 Sr and Nd isotope compositions of peridotitic cpx mineral separates and of the Labait host melilitite, as in Supplementary Table 1; averaged values (avg) shown in italics; ε_{Nd} is per 10,000 deviation from present-day chondrite (value of Wasserburg et al. 1981)

Sample	$^{87}Sr/^{86}Sr$	2se/2σ	$^{143}Nd/^{144}Nd$	2se/2σ	ε_{Nd}
Spinel-facies harzburgite					
LB-31 cpx	0.704158	0.000039	0.512196	0.000021	–8.6
Garnet-free harzburgite					
LB-21 cpx	0.704395	0.000021			
Garnet harzburgites and lherzolite					
KAT-17 cpx	0.703521	0.000020			
LB-4 cpx	0.703558	0.000021	0.512598	0.000042	–0.8
LB-4 cpx	0.703551	0.000025			
LB4-cpx avg	*0.703555*	*0.000010*			
LB-45 cpx	0.702951	0.000020	0.512862	0.000034	4.4
LB-45 cpx	0.702938	0.000030			
LB-45 cpx avg	*0.702945*	*0.000018*			
Fe-rich peridotites					
LB-46 cpx	0.704005	0.000020			
LB-51 cpx	0.705584	0.000027	0.512883	0.000028	4.8
Melilitite					
LB-2	0.705193	0.000021	0.512693	0.000018	1.1
LB-2	0.705154	0.000025	0.512676	0.000016	0.7
LB-2 avg	*0.705174*	*0.000055*	*0.512684*	*0.000024*	*0.9*

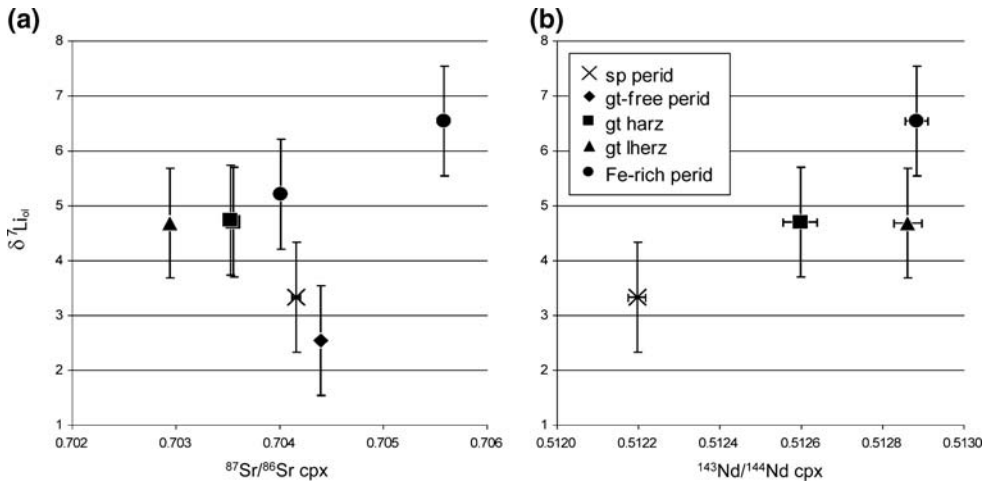

Fig. 4 **a** $^{87}Sr/^{86}Sr$ and **b** $^{143}Nd/^{144}Nd$ in cpx against δ^7Li in olivine from Labait

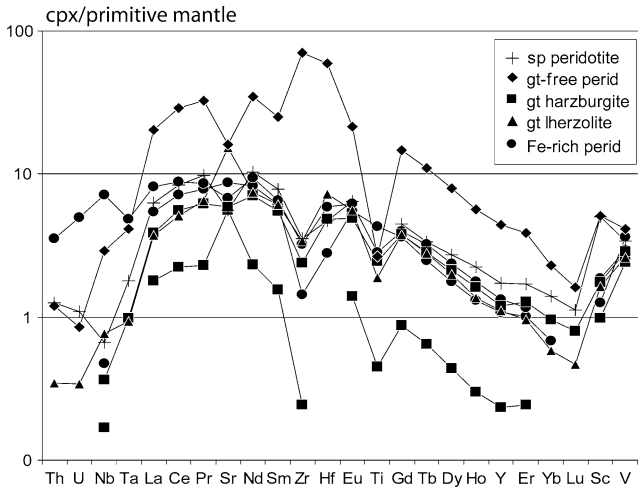

Fig. 5 Trace-element patterns of cpx in peridotites from Labait. Normalized to primitive mantle of McDonough and Sun (1995)

The systematic offset of δ^7Li between olivine and cpx in the Labait peridotites is in the same direction as that documented by some previous studies of mantle xenoliths (Seitz et al. 2004; Rudnick and Ionov 2007), with cpx systematically lighter than coexisting olivine. Whereas Seitz et al. (2004) found a maximum Δ^7Li^{ol-cpx} of ~3.5‰ and attributed this to equilibrium fractionation, Δ^7Li^{ol-cpx} of our samples ranges between 2 and 12. Similar and even larger fractionations (Δ^7Li^{ol-cpx} = 3–23) are reported by Rudnick and Ionov (2007) for olivine–clinopyroxene pairs from far-east Russian xenoliths, from some of the same localities investigated by Nishio et al. (2004), who documented unusually low δ^7Li_{cpx} (down to –17), but did not report any data for coexisting olivines. In contrast, other studies of peridotite xenoliths have found that Δ^7Li^{ol-cpx} ranges to both positive and negative values (–2.4 to +1.2‰, Magna et al. 2006; –3.6 to +13.5‰, Jeffcoate et al. 2007), and does not correlate with equilibration temperature. It is thus not clear whether measurable equilibrium fractionation exists between olivine and cpx at mantle temperatures, but it is apparent that minerals in the Labait peridotites are not in Li isotope equilibrium.

Interestingly, whereas Li concentrations appear to be equilibrated between olivine and cpx, Mg–Fe are not. The Mg number of cpx in the only two Fe-rich peridotites that contain this phase (LB-46 and LB-51) is much too high relative to that of coexisting olivine to be in equilibrium (Mg number cpx = 89.4 and 89.5 vs. Mg number olivine = 86.9 and 87.5, respectively, Fig. 6a, Supplementary Appendix 1). In contrast, these two samples fall on a correlation between Li in cpx and Fo content of coexisting olivines (Fig. 6b), but do not fall on a correlation between Li and Mg number in cpx (Fig. 6c). It thus appears that diffusion of Li in cpx is faster than Fe–Mg diffusion in cpx and at least as fast as Fe–Mg diffusion in olivine, such that the olivine Mg number reflects reaction with a metasomatic melt, whereas cpx does not (yet). This also means that the Li abundances of cpx are linked to the Fe and Li ingress seen in olivine. Furthermore, it suggests that the cpx Mg number in the Fe-rich peridotites records an older signature (higher Mg number), whereas olivine equilibrated with an infiltrating melt leading to lower Mg number, consistent with faster Fe–Mg diffusion in olivine relative to cpx (Klügel 2001). If so, the isotopic disequilibrium is not due to primary olivine being combined with secondary cpx crystallized from a melt. In fact, from textural evidence, only cpx in garnet-free peridotite LB-6 was considered to be secondary (Lee and Rudnick 1999).

Recent studies have suggested that Li diffusion in cpx is faster than in olivine (Jeffcoate et al. 2007; Rudnick and Ionov 2007; Parkinson et al. 2007). If so, the low δ^7Li_{cpx}

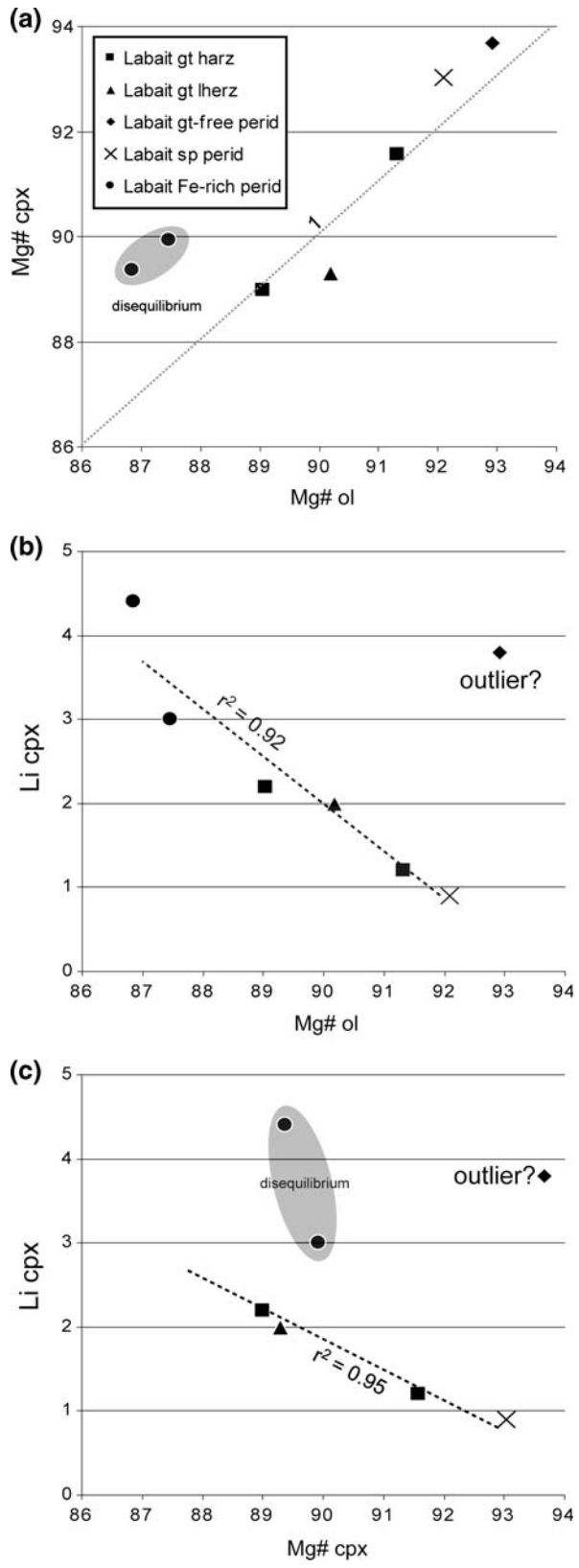

Fig. 6 **a** Mg number olivine against Mg number cpx, **b** Mg number olivine against Li concentration in cpx (ppm) and **c** Mg number cpx against Li concentration in cpx (ppm)

relative to δ^7Li_{ol} in the Labait peridotites, coupled with the lack of correlations between δ^7Li_{cpx} and other parameters, may reflect very recent diffusion of Li into cpx (but not olivine), and attendant kinetic isotope fractionation, possibly during transport in the melilitite host. Even small amounts of Li addition via diffusion from a grain-boundary source, such as the host melilitite, may produce large isotopic effects, while having little effect on overall concentration. The degree of isotopic fractionation is governed by the relative mobility of ^7Li and ^6Li, which relates to the exponent β, and the concentration contrast between the mineral and the source of Li (Richter et al. 2003). Modelling shows that for simple boundary conditions (one-dimensional diffusion in a semi-infinite medium of a 2 mm diameter sphere), using a diffusivity of Li in cpx of 10^{-11} m^2 s^{-1} (Coogan et al. 2005), β values of 0.19–0.27 (Parkinson et al. 2007) and a concentration contrast of 9 ppm (similar to that between the host melilitite and a 1 ppm Li cpx), total δ^7Li in the cpx decreases by ~5.7–8.2‰ in only ~5 min. At the same time, total Li concentration of the hypothetical cpx increases from 1 ppm to only 1.7 ppm. Thus, very recent Li addition to the cpx may have produced the observed isotopic disequilibria without strongly affecting the elemental partitioning between olivine and cpx.

The apparent Li elemental equilibrium between cpx and olivine for our sample suite suggests that this process was incipient, and had not lead to the significant Li enrichment and extreme isotope fractionation such as that seen in cpx in peridotites from far-east Russia (Rudnick and Ionov 2007). In this scenario, the δ^7Li_{cpx} is unrelated to the Li and Fe enrichment event evidenced by many Labait peridotites. We thus propose that, for the Labait samples, olivine best records the δ^7Li of the metasomatic agent responsible for the Fe-enrichment (giving rise to the correlations we see) and, due to its modal abundance, the δ^7Li of the whole rock. We thus focus the rest of our discussion on Li in olivine.

The Fe-enrichment event

The Li budget in mantle peridotite is controlled by olivine, which is the most abundant mineral and typically has Li concentrations (~1.6–1.9 ppm) that are slightly higher than those of coexisting pyroxenes (Ryan and Langmuir 1987; Brenan et al. 1998; Eggins et al. 1998; Seitz and Woodland 2000). Melt depletion leads to lower concentrations in all minerals, due to the moderate incompatibility of Li, whereas metasomatism leads to higher concentrations for the same reasons (e.g., Seitz and Woodland 2000). As mentioned above, most samples in our study have higher Li concentrations than olivine from primitive peridotites and thus probably experienced Li addition (Fig. 1a).

These elevated Li contents, combined with the correlations between δ^7Li and Li content (Fig. 1a), forsterite content and NiO in olivine (Fig. 2) suggest that the peridotites are the products of mixing between two components. One component is the ancient mantle lithosphere, which is refractory (Fe-poor) and isotopically light. The second component is an isotopically heavy, Li- and Fe-rich melt. The Re-enrichment seen these peridotites is likely also due to the same event (Chesley et al. 1999). If so, this event must represent an earlier phase of rift magmatism, since there is no correlation between Re-enrichment and Os isotope composition. Similar reaction between Li- and ^{7}Li-depleted lithospheric mantle with a Li-rich and isotopically heavy melt has been suggested for cratonic peridotites from southern Africa, but it is unclear whether the relatively light Li in ancient refractory mantle is due to earlier metasomatism or whether it reflects a secular evolution toward more isotopically heavy mantle due to addition of high-δ^7Li crustal components (Bell et al. 2005).

The Fe- and Li-rich and high-δ^7Li character of olivines in Fe-rich peridotites and the deep-seated garnet-bearing peridotites (including fertile garnet lherzolite, LB-45) are interpreted to be related to a prolonged metasomatic event involving plume-derived silicate melts associated with the EAR. It is likely that these peridotites, including cpx, have experienced metasomatic overprinting during earlier phases of rift magmatism. Indeed, the precipitation of Pleistocene zircons (Rudnick et al. 1999), coupled with enhanced Zr abundances on the rims of metasomatic rutiles in a vein from one of the ancient Labait harzburgites (Watson et al. 2006) suggests that this section of lithosphere has probably seen repeated injection of rift-related magmas over the last million years or so. A positive correlation between δ^7Li_{ol} and $^{143}Nd/^{144}Nd$ in cpx and a rough negative correlation between δ^7Li_{ol} and $^{87}Sr/^{86}Sr$ in cpx (Fig. 4a, with the exception of a single Fe-rich peridotite) would be consistent with mixing between a metasomatic component associated with the rift that has high $^{143}Nd/^{144}Nd$, low $^{87}Sr/^{86}Sr$ and heavy Li relative to the ancient, refractory mantle (Fig. 4b). In this context, the similarity of the cpx trace-element patterns (with the exception of highly incompatible elements Th, U, Nb and Ta, and Li abundances), in Fe-rich peridotites, garnet peridotites and spinel peridotite reflect interaction with similarly fractionated melts at different times (and depths) that could explain why the patterns are so similar, while at the same time the cpx have variable radiogenic isotope compositions.

In addition to identifying an ancient lithospheric mantle component and a rift component, another component is apparent in the lithospheric mantle beneath Tanzania. The single Fe-rich peridotite that plots off the $^{87}Sr/^{86}Sr$ in cpx vs. δ^7Li_{ol} trend (LB-51) has unusually radiogenic Sr relative to its mildly unradiogenic Nd, thus plotting in an unusual space on a $^{143}Nd/^{144}Nd$ vs. $^{87}Sr/^{86}Sr$ diagram (Fig. 7). Several lavas from the EAR (Macdonald et al. 2001), including the host melilitite measured here, plot in this area of the diagram, as do cpx from mantle xenoliths from Lashaine. These samples may reflect an exotic component present within the lithospheric mantle beneath Tanzania. Despite the complexities apparent in the radiogenic isotope data for Labait peridotites, we can conclude that the least radiogenic (with regard to Sr), plume-like isotope composition is observed for the most fertile, PM-like sample (LB-45), whose significance is discussed in the following section.

Sr-Nd-Li isotope composition of the East African plume

Estimating the isotopic composition of a plume from derivative lavas erupted through ancient lithosphere can be difficult because the lavas may interact with and become contaminated by isotopically evolved lithospheric crust and mantle during ascent, as demonstrated previously for lavas of the EAR (e.g., Paslick et al. 1995; Bell and Simonetti 1996; Macdonald et al. 2001). Samples from the lithospheric mantle that have been metasomatized by plume-

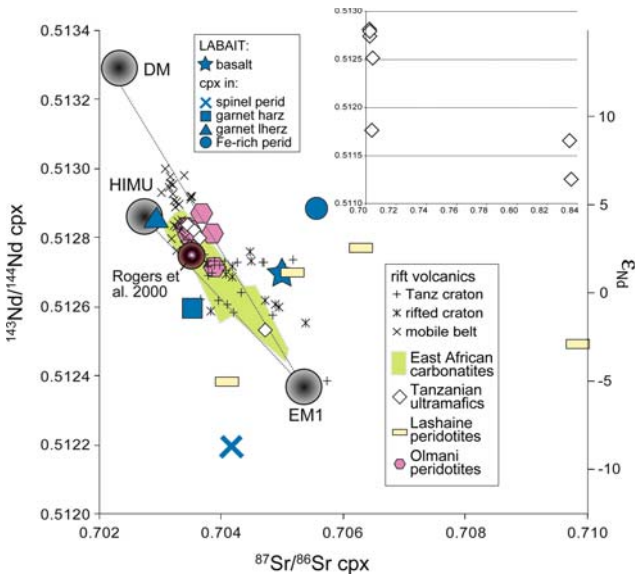

Fig. 7 $^{87}Sr/^{86}Sr$-$^{143}Nd/^{144}Nd$ (ε_{Nd} on *right axis*) correlation diagram for cpx mineral separates and melilitite from Labait. Olmani peridotites from Rudnick et al. (1993); Lashaine peridotites (authors' unpublished data); field for East African carbonatites, DM, HIMU and EMI mantle end-members from Bell and Tilton (2001); Kenya rift volcanics (divided into those penetrating the Tanzanian craton, the rifted craton and the mobile belt) from Macdonald et al. (2001) and estimated plume composition from Rogers et al. (2000); Tanzanian ultramafics from Cohen et al. (1984), inset shows extended diagram including samples with extremely radiogenic Sr

derived melts, as postulated for Labait peridotites (Lee and Rudnick 1999), may better reflect the isotopic affinity of the plume, provided their trace-element inventory has been sufficiently overprinted. This is obviously not the case for peridotites with evolved Sr and Nd and unradiogenic Os isotope compositions (Chesley et al. 1999), such as the shallow and ancient peridotites from Labait (spinel-facies and garnet-free peridotites, as well as the one Fe-rich peridotite that sits at high Sr relative to Nd (LB-51), discussed above). The host melilitite (LB-2) also appears to have acquired an anomalously high $^{87}Sr/^{86}Sr$ signature during passage through the lithospheric mantle (Table 2, Fig. 7).

In contrast, the isotopic composition of the plume feeding the EAR may be deduced from the samples that show the greatest overprinting by rift-related magmas [Fe-rich peridotites and the high-temperature fertile lherzolite (LB-45)]. The latter sample is derived from the lithosphere–asthenosphere boundary (ca 1,400°C equilibration temperature), where it was heavily overprinted by plume-derived asthenospheric melts, and it has a highly unusual major-element composition for cratonic peridotite that is similar to primitive upper mantle estimates (Lee and Rudnick 1999). It contains radiogenic $^{187}Os/^{188}Os$ that is similar to that of the host melilitite and a glimmerite (LB-49) that are believed to represent those of the plume-like asthenospheric mantle (Chesley et al. 1999), and its non-mantle-like PGE concentrations and evidence for the presence of multiple Os isotope components are consistent with such overprinting (Becker et al. 2006).

Even though at first glance Fe-rich peridotites (FeO 11.2–14.1 wt%) seem to have experienced a higher degree of melt infiltration than fertile peridotite LB-45 (FeO 8.3 wt%), they likely formed by melt-rock reaction between asthenosphere (plume)-derived melts and lithospheric mantle. This would lead to decreasing MgO and NiO contents in the residual melt without affecting the relative abundances of most other elements, in accord with the lower MgO and NiO contents in the Fe-rich peridotites. In contrast, LB-45 is suggested to have reacted with a "primitive" asthenospheric melt close to the lithosphere–asthenosphere boundary.

Although we did not measure $^{206}Pb/^{204}Pb$, which defines the HIMU mantle reservoir, the Sr-Nd isotope composition of LB-45 (0.7029 and 0.5129, respectively) is similar to HIMU (Fig. 7), and we suggest that this value is likely to best reflect the Sr and Nd isotopic composition of the plume feeding this portion of the EAR. This is supported by the HIMU-like isotopic compositions of some carbonatites and mafic lavas from Tanzania and Kenya (Paslick et al. 1995; Bell and Simonetti 1996; Macdonald et al. 2001; Bell and Tilton 2001; Furman et al. 2006). Because LB-45 is derived from the base of the lithosphere, and its bulk rock composition has been very strongly overprinted, its HIMU signature is proposed to have a sublithospheric origin (like the lavas from Turkana, Kenya, Furman et al. 2006), rather than originating in ancient enriched continental lithospheric mantle, as proposed by Paslick et al. (1995) for a number of the Tanzanian rift-related lavas.

The Fe-rich peridotites from Labait form one end-member of the lithium mixing line (Figs. 1a, 2), with δ^7Li up to +6.6. These rocks are suggested to have formed by rift-related melt-rock reaction (Lee and Rudnick 1999; Chesley et al. 1999), thus their Li isotope composition likely represents that of the source of the rift basalts. The fertile garnet peridotite that was used to define the Sr and Nd composition of the plume beneath Labait, LB-45, has a slightly lower δ^7Li (+4.7), although within uncertainty (±1‰) of the Fe-rich peridotites. Collectively, these data suggest that the plume source of the rift basalts in Tanzania has a heavy lithium isotope composition similar, though not exclusive to OIBs with HIMU affinity (δ^7Li up to +7; Jeffcoate and Elliott 2003; Ryan and Kyle 2004; Nishio et al. 2005).

Plume vs. lithosphere signatures

The approach taken above, to define the EAR plume composition from mantle xenoliths that either formed directly from, or were strongly overprinted by rift-related magmas, can be extended to localities beyond Labait. Clinopyroxenes in dunites and wehrlites from the Olmani volcano, northern Tanzania, formed by rift-related carbonatite overprint of ancient refractory mantle lithosphere (Rudnick et al. 1993). These peridotites have highly variable parent–daughter ratios, yet remarkably homogeneous $^{87}Sr/^{86}Sr$ (0.7034–0.7039) and $^{143}Nd/^{144}Nd$ (0.51281–0.51283) that fall between the HIMU and EMI components. The isotopic homogeneity at this locality, despite highly variable parent–daughter ratios, indicates that the metasomatism was recent and that the carbonatitic melt effectively overprinted any original isotopic signature of these rocks (Rudnick et al. 1993). In contrast, the plume beneath Labait is inferred to have HIMU-affinity based on the Labait peridotites described above (see Sect. "Sr-Nd-Li isotope composition of the East African plume").

The small but significant difference in Sr-Nd isotope composition of samples considered to best represent the plume component at Labait and at Olmani, respectively, which are located within ~150 km of each other, may point to isotopic heterogeneity in the plume. Plume heterogeneity has been suggested for carbonatites that are located at a similar distance from each other beneath the Kenya rift and that show HIMU and EMI affinities, respectively (Bell and Tilton 2001).

It is also possible that the EMI component in the metasomatic carbonatite from Olmani was acquired during percolation of the melt through metasomatized mantle (e.g., Bell and Simonetti 1996), rather than indicating true plume heterogeneity. For example, rift-related volcanic rocks from northern Tanzania have OIB-like trace-element compositions, whereas their isotopic compositions, in particular unradiogenic Nd, were suggested to point to a lithospheric mantle source that has been enriched by small-volume melts (Paslick et al. 1995). In addition, the low δ^7Li of +3.4 for a primitive olivine–melilitite from the nearby Oldoinyo Lengai carbonatite volcano (Halama et al. 2007), similar to refractory LREE-enriched spinel peridotite LB-31 (+3.3, see Sect. "The Fe-enrichment event"), may reflect assimilation of ancient refractory metasomatized mantle by the olivine–melilitite, or a lithospheric source.

We argue that the convergence of Sr-Nd isotope systematics for different materials and localities (carbonatite-metasomatized peridotites from Olmani; Rudnick et al. 1993; authors' unpublished Data; ankaramite, peridotitic cpx and vein material from Pello Hill and Eledoi; Cohen et al. 1984) suggests that a ^{143}Nd/^{144}Nd of ~0.51280–0.51284 and ^{87}Sr/^{86}Sr of ~0.7034–0.7035 expresses the plume characteristics beneath some regions of Tanzania, while beneath Labait the plume may be more HIMU-like. The uniformity of Sr-Nd isotope ratios from Olmani are all the more striking as the mantle beneath Tanzania has been variably and unsystematically metasomatized (Macdonald et al. 2001; Dawson 2002).

The Sr-Nd isotope compositions of peridotites from Labait and Olmani differ slightly from the common end-member for Neogene to Recent basalts that has a more radiogenic ^{143}Nd/^{144}Nd of ~0.51275 and ^{87}Sr/^{86}Sr of ~0.7035 and that has been suggested to represent the isotopic composition of the plume beneath the Kenya Rift, which comprises the area between Turkana and northern Tanzania (Rogers et al. 2000). Recently, the plume generating volcanism in Turkana and Afar, north of Tanzania, has been proposed to be heterogeneous, containing lenses of isotopically distinct materials (Furman et al. 2006) and our data suggest that this may also be true for the plume beneath Tanzania.

Summary and conclusions

The δ^7Li of peridotitic olivine, combined with ^{87}Sr/^{86}Sr and ^{143}Nd/^{144}Nd of coexisting cpx are used to unravel the rift-related and pre-rift history of the lithospheric mantle beneath the Tanzanian craton margin (Labait) and to place constraints on the composition of the plume feeding the Tanzanian section of the EAR:

(1) Addition of Fe and isotopically heavy Li is inferred from positive correlations between Li, δ^7Li and FeO of olivine in peridotites from Labait that are proposed to have interacted with plume-derived silicate melts (Lee and Rudnick 1999; Chesley et al. 1999).
(2) A fertile, high-temperature garnet lherzolite with radiogenic Os, inferred to have been entrained from close to the lithosphere–asthenosphere boundary, may best represent the composition of the plume component beneath Labait (Lee and Rudnick 1999; Chesley et al. 1999). It has Sr-Nd isotope compositions (^{87}Sr/^{86}Sr = 0.7029 and ^{143}Nd/^{144}Nd = 0.51286) similar to the HIMU mantle reservoir, which is an end-member in EAR-related volcanism. This is slightly less evolved than a previous estimate for the plume beneath the rift (0.70354 and 0.51275, respectively; Rogers et al. 2000) and may reflect plume heterogeneity or, alternatively, point to assimilation of old metasomatised mantle for the latter estimate, which is based on rift-related lavas.
(3) The Fe- and Li-rich peridotites have δ^7Li of +5.2 to +6.6. These, along with the deep-seated garnet lherzolite, which has a δ^7Li of +4.7, may best represent the Li isotope composition of the EAR plume beneath Labait, which is isotopically heavy, lying near the high end of estimates for MORB and overlapping with previous estimates of the δ^7Li of HIMU oceanic basalts.

Acknowledgments Jay Kaufman, Igor Puchtel and Rich Walker are thanked for sharing their expertise in the isotope geochemistry lab and with the TIMS, Michael Marks and Fang-zhen Teng for advice regarding Li chemistry, Richard Ash for assistance on the ELEMENT 2 ICPMS and Nu MC-ICPMS and Dave Bell for stimulating discussion. The insightful and constructive comments of Thomas Zack and one anonymous reviewer, and editorial handling by J. Hoefs, are gratefully acknowledged. This work was carried out with support from the NSF (grants EAR 0208012 and 0609689) and while S.A. was the recipient of a Feodor-Lynen fellowship from the Alexander-von-Humboldt Foundation.

References

Barth MG, Rudnick RL, Horn I, McDonough WF, Spicuzza MJ, Valley JW, Haggerty SE (2001) Geochemistry of xenolithic eclogites from West Africa, Part I: a link between low MgO eclogites and Archean crust formation. Geochim Cosmochim Acta 65:1499–1527

Becker H, Horan MF, Walker RJ, Gao S, Lorand J-P, Rudnick RL (2006) Highly siderophile element composition of the Earth's primitive upper mantle: constraints from new data on peridotite massifs and xenoliths. Geochim Cosmochim Acta 70:4528–4550

Bell K, Simonetti A (1996) Carbonatite magmatism and plume activity: implications from the Nd, Pb and Sr isotope systematics of Oldoinyo Lengai. J Petrol 37:1321–1339

Bell K, Tilton GR (2001) Nd, Pb and Sr isotopic compositions of east African carbonatites: evidence for mantle mixing and plume inhomogeneity. J Petrol 42:1927–1945

Bell DR, Hervig RL, Buseck PR (2005) Li-isotope studies of olivine in mantle xenoliths by SIMS. Abstract, Lunar and Planetary Science XXXVI, League City

Benton LD, Ryan JG, Savov IP (2004) Lithium abundance and isotope systematics of forearc serpentinites, Conical Seamount, Mariana forearc: insights into the mechanics of slab-mantle exchange during subduction. Geochem Geophys Geosyst 5:Q08J12. doi:10.1029/2004GC000708

Bouman C, Elliott T, Vroon PZ (2004) Lithium inputs to subduction zones. Chem Geol 212:59–79

Brenan JM, Neroda E, Lundstrom CC, Shaw HF, Ryerson FJ, Phinney DL (1998) Behaviour of boron, beryllium, and lithium during melting and crystallization: constraints from mineral-melt partitioning experiments. Geochim Cosmochim Acta 62:2129–2141

Burton KW, Schiano P, Birck JL, Allegre CJ, Rehkämper M, Halliday AN, Dawson JB (2000) The distribution and behaviour of rhenium and osmium amongst mantle minerals and the age of the lithospheric mantle beneath Tanzania. Earth Planet Sci Lett 183:93–106

Chan LH, Edmond JM, Thompson G, Gillis K (1992) Lithium isotopic composition of submarine basalts: implications for the lithium cycle in the oceans. Earth Planet Sci Lett 108:151–160

Chan LH, Alt JC, Teagle DAH (2002) Lithium and lithium isotope profiles through the upper oceanic crust: a study of seawater-basalt exchange at ODP Sites 504B and 896A. Earth Planet Sci Lett 201:187–201

Chesley JT, Rudnick RL, Lee CT (1999) Re-Os systematics of mantle xenoliths from the East African Rift: age, structure, and history of the Tanzanian craton. Geochim Cosmochim Acta 63:1203–1217

Cohen RS, O'Nions RK, Dawson JB (1984) Isotope geochemistry of xenoliths from East Africa: implications for development of mantle reservoirs and their interaction. Earth Planet Sci Lett 68:209–220

Coogan LA, Kasemann SA, Chakraborty S (2005) Rates of hydrothermal cooling of new oceanic upper crust derived from lithium-geospeedometry. Earth Planet Sci Lett 240:415–424

Dawson JB (1984) Contrasting types of mantle metasomatism? In: Kornprobst J (ed) Kimberlites II: the mantle and crust-mantle relationships. Elsevier, Amsterdam, pp 289–294

Dawson JB (1992) Neogene tectonics and volcanicity in the North Tanzania sector of the Greogory Rift-Valley—contrasts with the Kenya sector. Tectonophysics 204:81–92

Dawson JB (1999) Metasomatism and melting in spinel peridotite xenoliths from Labait, Tanzania. In: Gurney J, Gurney J, Pascoe M, Richardson S (eds) Proceedings of the 7th International Kimberlite Conference, Red Roof Design cc, Cape Town, pp 164–173

Dawson JB (2002) Metasomatism and partial melting in upper-mantle peridotite xenoliths from the Lashaine volcano, Northern Tanzania. J Petrol 43:1749–1777

Ebinger C, Bechtel C, Forsyth D, Bowin C (1989) Effective elastic plate thickness beneath the east African and Afar plateaus and dynamic compensation for the uplifts. J Geophys Res 94:2883–2901

Eggins SM, Rudnick RL, McDonough WF (1998) The composition of peridotites and their minerals: a laser-ablation ICP-MS study. Earth Planet Sci Lett 154:53–71

Flesch GD, Anderson AR Jr, Svec HJ (1973) A secondary isotopic standard for $^{6}Li/^{7}Li$ determinations. Int J Mass Spectrom Ion Phys 12:265–272

Furman T, Kaleta KM, Bryce JG, Hanan BB (2006) Tertiary Mafic Lavas of Turkana, Kenya: constraints on East African plume structure and the occurrence of high-μ volcanism in Africa. J Petrol 47:1221–1244

George R, Rogers N, Kelley S (1998) Earliest magmatism in Ethiopia: evidence for two mantle plumes in one flood basalt province. Geology 26:923–926

Gurenko AA, Schmincke HU (2002) Orthopyroxene-bearing tholeiites of the Iblean Plateau (Sicily): constraints on magma origin and evolution from glass inclusions in olivine and orthopyroxene. Chem Geol 183:305–331

Halama R, McDonough WF, Rudnick RL, Keller J, Klaudius J (2007) The Li isotopic composition of Oldoinyo Lengai: nature of the mantle sources and lack of isotopic fractionation during carbonatite petrogenesis. Earth Planet Sci Lett 254:77–89

James RH, Palmer MR (2000) The lithium isotope composition of international rock standards. Chem Geol 166:319–326

Jeffcoate AB, Elliott T (2003) Tracing recycled Li in the mantle: insights into mantle heterogeneities. EOS Trans AGU 84:V52A–0416

Jeffcoate AB, Elliott T, Thomas A, Bouman C (2004) Precise, small sample size determinations of lithium isotopic compositions of geological reference materials and modern seawater by MC-ICP-MS. Geostand Geoanal Res 28:161–172

Jeffcoate AB, Elliott T, Kasemann SA, Ionov D, Cooper K, Brooker R (2007) Li isotope fractionation in peridotites and mafic melts. Geochim Cosmochim Acta 71:202–218

Klügel A (2001) Prolonged reactions between harzburgite xenoliths and silica-undersaturated melt: implications for dissolution and Fe-Mg interdiffusion rates of orthopyroxene. Contrib Mineral Petrol 141:1–14

Kobayashi K, Tanaka R, Moriguti T, Shimizu K, Nakamura E (2004) Lithium, boron and lead isotope systematics of glass inclusions in olivines from Hawaiian lavas: evidence for recycled components in the Hawaiian plume. Chem Geol 212:143–161

Latin D, Norry MJ, Tarzey RJE (1993) Magmatism in the Gregory Rift, East-Africa—evidence for melt generation by a plume. J Petrol 34:1007–1027

Lee C-T, Rudnick RL (1999) Compositionally stratified cratonic lithosphere: petrology and geochemistry of peridotite xenoliths from the Labait volcano, Tanzania. In: Gurney J, Gurney J, Pascoe M, Richardson S (eds) Proceedings of the 7th international Kimberlite conference. Red Roof Design cc, Cape Town, pp 503–521

Macdonald R, Rogers NW, Fitton JG, Black S, Smith M (2001) Plume–lithosphere interactions in the generation of the basalts of the Kenya Rift, East Africa. J Petrol 42:877–900

Magna T, Wiechert UH, Halliday AN (2004) Low-blank isotope ratio measurement of small samples of lithium using multiple-collector ICPMS. Int J Mass Spectrom 239:67–76

Magna T, Wiechert UH, Halliday AN (2006) New constraints on the lithium isotope compositions of the Moon and terrestrial planets. Earth Planet Sci Lett 243:336–353

Marty B, Pik R, Gezahegn Y (1996) Helium isotopic variations in Ethiopian plume lavas: nature of magmatic sources and limit on lower mantle contribution. Earth Planet Sci Lett 144:223–237

McDonough WF, Sun S-S (1995) The composition of the Earth. Chem Geol 120:223–253

Möller A, Mezger K, Schenk V (1998) Crustal age domains and the evolution of the continental crust in the Mozambique Belt of Tanzania: combined Sm-Nd, Rb-Sr, and Pb-Pb isotopic evidence. J Petrol 39:749–783

Moriguti T, Nakamura E (1998) High-yield lithium separation and precise isotopic analysis for natural rock and aqueous samples. Chem Geol 145:91–104

Nishio Y, Nakai S, Yamamoto J, Sumino H, Matsumoto T, Prikhod'ko VS, Arai S (2004) Lithium isotopic systematics of the mantle-derived ultramafic xenoliths: implications for EMI origin. Earth Planet Sci Lett 217:245–261

Nishio Y, Nakai S, Kogiso T, Barsczus HG (2005) Lithium, strontium, and neodymium isotopic compositions of oceanic island basalts in the Polynesian region: constraints on a Polynesian HIMU origin. Geochem J 39:91–103

Paquin J, Altherr R (2002) Subduction-related lithium metasomatism during exhumation of the Alpe Arami ultrahigh-pressure garnet peridotite (Central Alps, Switzerland). Contrib Mineral Petrol 143:623–640

Parkinson IJ, Hammond SJ, James RH, Rogers NW (2007) High-temperature lithium isotope fractionation: insights from lithium isotope diffusion in magmatic systems. Earth Planet Sci Lett 257:609–621

Paslick C, Halliday A, James D, Dawson JB (1995) Enrichment of the continental lithosphere by OIB melts: isotopic evidence from the volcanic province of northern Tanzania. Earth Planet Sci Lett 130:109–126

Raczek I, Jochum KP, Hofmann AW (2003) Neodymium and strontium isotope data for USGS reference materials BCR-1, BCR-2, BHVO-1, BHVO-2, AGV-1, AGV-2, GSP-1, GSP-2 and eight MPI-DING reference glasses. Geostand Newsl 27:173–179

Richter FM, Davis AM, DePaolo DJ, Watson EB (2003) Isotope fractionation by chemical diffusion between molten basalt and rhyolite. Geochim Cosmochim Acta 67:3905–3923

Rogers N, Macdonald R, Fitton JG, George R, Smith M, Barreiro B (2000) Two mantle plumes beneath the East African rift system: Sr, Nd and Pb isotope evidence from Kenya Rift basalts. Earth Planet Sci Lett 176:387–400

Rudnick RL, Ionov DA (2007) Lithium elemental and isotopic disequilibrium in minerals from peridotite xenoliths from far-east Russia: product of recent melt/fluid-rock reaction. Earth Planet Sci Lett 256:278–293

Rudnick RL, McDonough WF, Orpin A (1992) Northern Tanzanian peridotite xenoliths: a comparison with Kaapvaal peridotites and inferences on metasomatic interactions. In: Meyer HOA, Leonardos O (eds) Kimberlites, related rocks and mantle xenoliths. Proceedings of the 5th international Kimberlite conference, vol I, pp 336–353

Rudnick RL, McDonough WF, Chappell BW (1993) Carbonatite metasomatism in the northern Tanzanian mantle: petrographic and geochemical characteristics. Earth Planet Sci Lett 114:463–475

Rudnick RL, Ireland TR, Gehrels G, Irving AJ, Chesley JT, Hanchar JM (1999) Dating mantle metasomatism: U-Pb geochronology of zircons in cratonic mantle xenoliths from Montana and Tanzania. In: Gurney J, Gurney J, Pascoe M, Richardson S (eds) Proceedings of the 7th international Kimberlite conference. Red Roof Design cc, Cape Town, pp 728–735

Rudnick RL, Tomascak PB, Njo HB, Gardner LR (2004) Extreme lithium isotopic fractionation during continental weathering revealed in saprolites from South Carolina. Chem Geol 212:45–57

Ryan JG, Langmuir CH (1987) The systematics of lithium abundances in young volcanic rocks. Geochim Cosmochim Acta 51:1727–1741

Ryan JG, Kyle PR (2004) Lithium abundance and lithium isotope variations in mantle sources: insights from intraplate volcanic rocks from Ross Island and Marie Byrd Land (Antarctica) and other oceanic Islands. Chem Geol 212:125–142

Scambelluri M, Hermann J, Morten L, Rampone E (2006) Melt- versus fluid-induced metasomatism in spinel to garnet wedge peridotites (Ulten Zone, Eastern Italian Alps): clues from trace element and Li abundances. Contrib Mineral Petrol 151:372–394

Seitz HM, Woodland AB (2000) The distribution of lithium in peridotitic and pyroxenitic mantle lithologies—an indicator of magmatic and metasomatic processes. Chem Geol 166:47–64

Seitz HM, Brey GP, Lahaye Y, Durali S Weyer S (2004) Lithium isotopic signatures of peridotite xenoliths and isotopic fractionation at high temperature between olivine and pyroxenes. Chem Geol 212:163–177

Smith M, Mosley P (1993) Crustal heterogeneity and basement influence on the development of the Kenya Rift, East Africa. Tectonics 12:591–606

Tanaka T, Togashi S, Kamioka H, Amakawa H, Kagami H, Hamamoto T, Yuhara M, Orihashi Y, Yoneda S, Shimizu H, Kunimaru T, Takahashi K, Yanagi T, Nakano T, Fujimaki H, Shinjo R, Asahara Y, Tanimizu M, Dragusanu C (2000) JNdi-1: a neodymium isotopic reference in consistency with LaJolla neodymium. Chem Geol 168:279–281

Teng F-Z, McDonough WF, Rudnick RL, Dalpé C, Tomascak PB, Chappell BW, Gao S (2004) Lithium isotopic composition and concentration of the upper continental crust. Geochim Cosmochim Acta 68:4167–4178

Teng F-Z, McDonough WF, Rudnick RL, Walker RJ (2006) Diffusion-driven extreme lithium isotopic fractionation in country rocks of the Tin Mountain pegmatite. Earth Planet Sci Lett 243:701–710

Thirlwall MF (1991) Long-term reproducibility of multicollector Sr and Nd isotope ratio analysis. Chem Geol 94:85–104

Tomascak PB, Tera F, Helz RT, Walker RJ (1999) The absence of lithium isotope fractionation during basalt differentiation: new measurements by multicollector sector ICP-MS. Geochim Cosmochim Acta 63:907–910

Vauchez A, Dineur F, Rudnick R (2005) Microstructure, texture and seismic anisotropy of the lithospheric mantle above a mantle plume: insights from the Labait volcano xenoliths (Tanzania). Earth Planet Sci Lett 232:295–314

Wasserburg GJ, Jacobsen SB, DePaolo DJ, McCulloch MT, Wen T (1981) Precise determination of Sm/Nd ratios, Sm and Nd isotopic abundances in standard solutions. Geochim Cosmochim Acta 45:2311–2323

Watson EB, Wark DA, Thomas JB (2006) Crystallization thermometers for zircon and rutile. Contrib Mineral Petrol 151:413–433

Weeraratne DS, Forsythe DW, Fischer KM, Nyblade AA (2003) Evidence for an upper mantle plume beneath the Tanzanian craton from Rayleigh wave tomography. J Geophys Res 108:2427

Wunder B, Meixner A, Romer RL, Heinrich W (2006) Temperature-dependent isotopic fractionation of lithium between clinopyroxene and high-pressure hydrous fluids. Contrib Mineral Petrol 151:112–120

Zack T, Tomascak PB, Rudnick RL, Dalpé C, McDonough WF (2003) Extremely light Li in orogenic eclogites: the role of isotope fractionation during dehydration in subducted oceanic crust. Earth Planet Sci Lett 208:209–290